Comparison of Supercell Maintenance and Dissipation Processes Observed During VORTEX2

NC STATE UNIVERSITY

Casey E. Letkewicz and Matthew D. Parker

Convective Storms Group, Department of Marine, Earth, and Atmospheric Sciences, North Carolina State University

Introduction

The developing and mature stages of supercells have been studied extensively, with their basic dynamical processes relatively well-understood (e.g., Rotunno and Klemp 1982; Davies-Jones 1984; Rotunno and Klemp 1985; Brandes 1988; Weisman and Rotunno 2000; Davies-Jones 2002). However, significantly fewer studies have been conducted on the processes associated with the dissipating stage of supercells (e.g., Bluestein 2008; Ziegler et al. 2010).

Over the course of the VORTEX2 field campaign, observations were collected on two dissipating supercells (9 June 2009 and 15 May 2010) and one elevated supercell that persisted for a number of hours (6 May 2010). In order to achieve a more complete understanding of the intricacies of supercell maintenance, this study compares the environments and evolution of the three different cases. The long-range goal of this study is to further our understanding of the key processes associated with dissipation and assess their relative contributions.

Analysis Methods

- Time-to-space conversion of quality-controlled, bias-corrected mobile mesonet and StickNet data
- Dual-Doppler synthesis
  - → Multi-pass Barnes scheme, interpolated onto grid (horizontal and vertical grid spacing between 250 and 500 m)
  - → Smoothing parameter κ based on recommendations of Pauley and Wu (1990) and Trapp and Doswell (2000)
  - → Advection based on storm motion estimated from WSR-88D tracking algorithm
  - → 3D wind syntheses constructed using upward integration
- Mobile soundings which did not reach the tropopause were modified using the nearest sounding in time and space for consistent calculations of CAPE and CIN

Case Selection

- 9 June 2009 (dissipating supercell)
  - → Supercell formed just north of a remnant outflow boundary and developed strong low-level rotation, but dissipated as it moved deeper into the cool air
- 6 May 2010 (elevated supercell)
  - → Supercell formed above a stable post-frontal airmass and persisted for several hours
- 15 May 2010 (dissipating supercell)
  - → Supercell developed orographically but weakened as it moved off of the terrain and into a more capped environment
- Key questions from these cases: *Under what conditions will a storm become elevated versus dissipate? What processes are important?*

→ *9 June 2009 (dissipating supercell)*

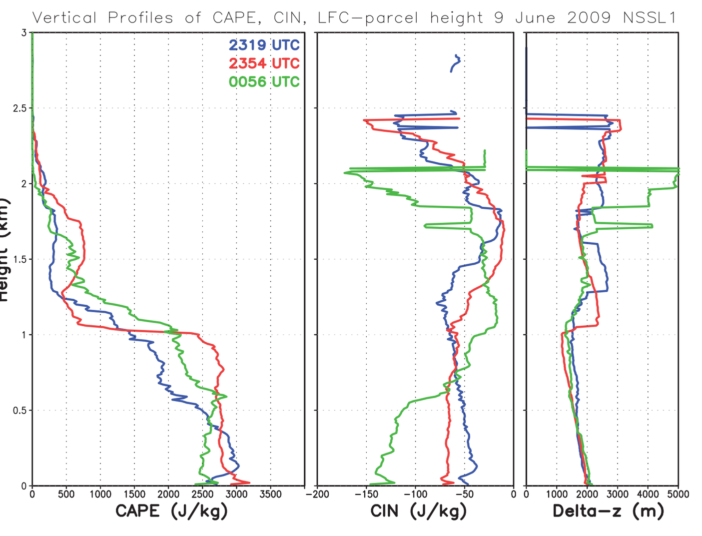

Fig. 1: Vertical profiles of CAPE, CIN, and delta-z (vertical distance between the parcel height and level of free convection) over time from the NSSL1 inflow soundings on 9-10 June 2009.

Near Inflow

	2319 UTC	2354 UTC	0056 UTC
0-6 km shear (m/s)	32.0	29.0	24.2
0-3 km shear (m/s)	14.8	17.7	20.0
0-1 km shear (m/s)	1.8	5.7	5.9
Effective shear (m/s)	18.7	19.5	11.2
0-3 km SRH (m²/s²)	319	277	124
0-1 km SRH (m²/s²)	47	53	-7
Effective SRH (m²/s²)	273	215	68
Effective layer depth (m)	2120	2130	1910

Table 1: Shear and SRH parameters computed from the NSSL1 inflow soundings on 9 June 2009. Shear parameters were calculated using the bulk shear vector magnitude for the appropriate layer. Effective parameters were defined as the layer were CAPE ≥ 100 J/kg and CIN ≥ -250 J/kg (as in Thompson et al. 2007). Near inflow refers to the region approximately 30 km downstream of the updraft.

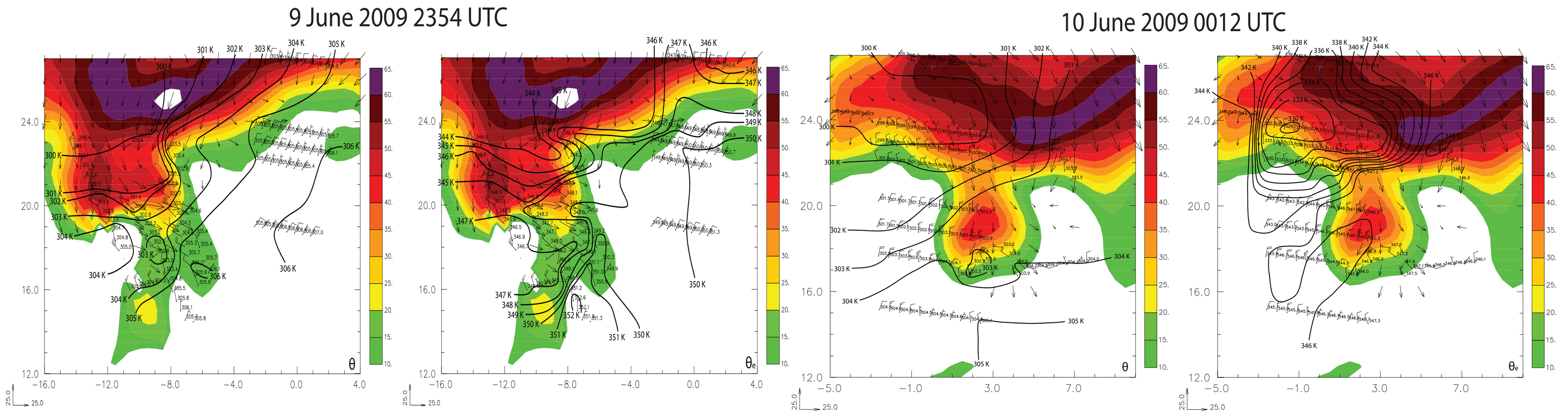

Fig. 2: Plan view of radar reflectivity and ground-relative wind vectors (500 m above the surface; derived from SMART-R dual-Doppler syntheses) at 2354 and 0012 UTC overlaid with time-to-space coverted mobile mesonet and Sticknet tracks. Each track is three minutes in length. Thermodynamic fields (θ or θe, as labeled) are subjectively analyzed and contoured. The x- and y-axes represent distance in km from the center of the grid (which is the position of SMART-R1).

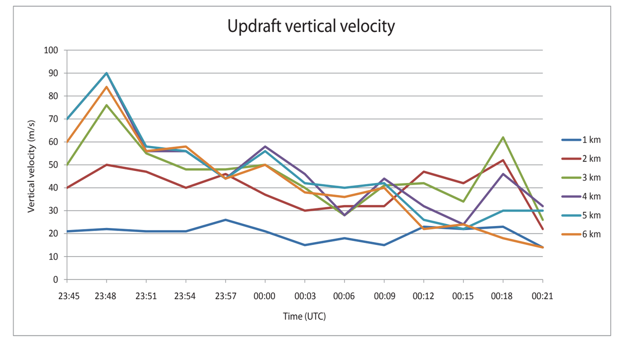

Fig. 3: Time series of dual-Doppler-derived (using SMART-R1 and SMART-R2) maximum updraft vertical velocities at several heights from 9 June 2009.

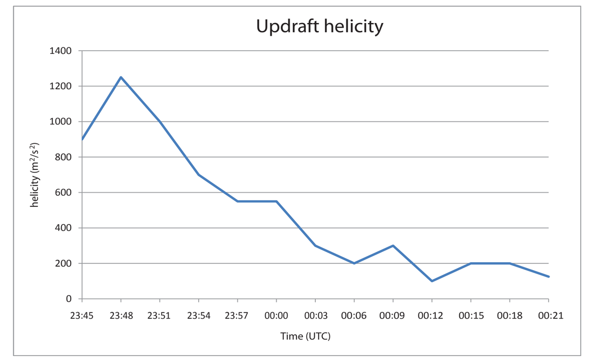

Fig. 4: Time series of dual-Doppler-derived (using SMART-R1 and SMART-R2) updraft helicity (m²/s²) from 9 June 2009, calculated as in Kain et al. (2008).

- Inflow environment had increasingly stable low-levels, but maintained favorable elevated conditions with sufficient CAPE & decreasing CIN that storm could have continued to feed on given sufficient lifting (Fig. 1)
- Strong decreases in shear and helicity (Table 1) could impact updraft strength and rotation (Figs. 3-4) via weaker dynamic lifting, a smaller flux of horizontal streamwise vorticity tilted into the updraft, and changes to cold pool-shear interactions, affecting lifting by the cold pool
  - → Low-level lifting also influenced by the cooling surface, resulting in weaker temperature gradients (Fig. 2)

→ *6 May 2010 (elevated supercell)*

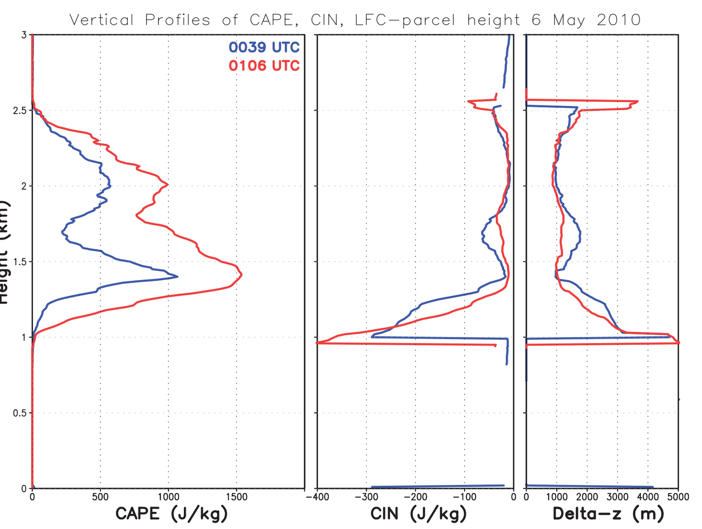

Fig. 5: As in Fig. 1, but for the inflow soundings launched on 7 May 2010.

	Near Inflow	*Far Inflow*
	0039 UTC	0106 UTC
0-6 km shear (m/s)	32.0	35.5
0-3 km shear (m/s)	15.8	14.2
0-1 km shear (m/s)	10.1	12.0
Effective shear (m/s)	16.6	20.1
0-3 km SRH (m²/s²)	548	747
0-1 km SRH (m²/s²)	36	167
Effective SRH (m²/s²)	312	385
Effective layer depth (m)	1210	1360

Table 2: As in Table 1, but for the inflow soundings launched on 7 May 2010. The near inflow region is defined as in Table 1, with the far inflow region located approximately 100 km downstream of the updraft.

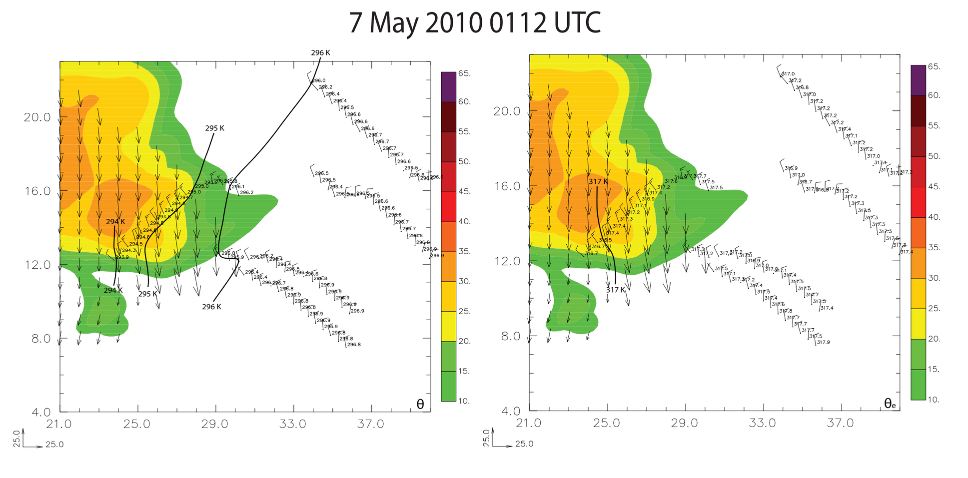

Fig. 6: As in Fig. 2, but at 0112 UTC 7 May 2010. Dual-Doppler winds are 250 m above the ground and were derived using the DOW6 and DOW7 radars. Due to a calibration error, reflectivities are approximately 20 dBZ too low. The x- and y-axes represent distance in km from the center of the grid (which is the position of DOW7).

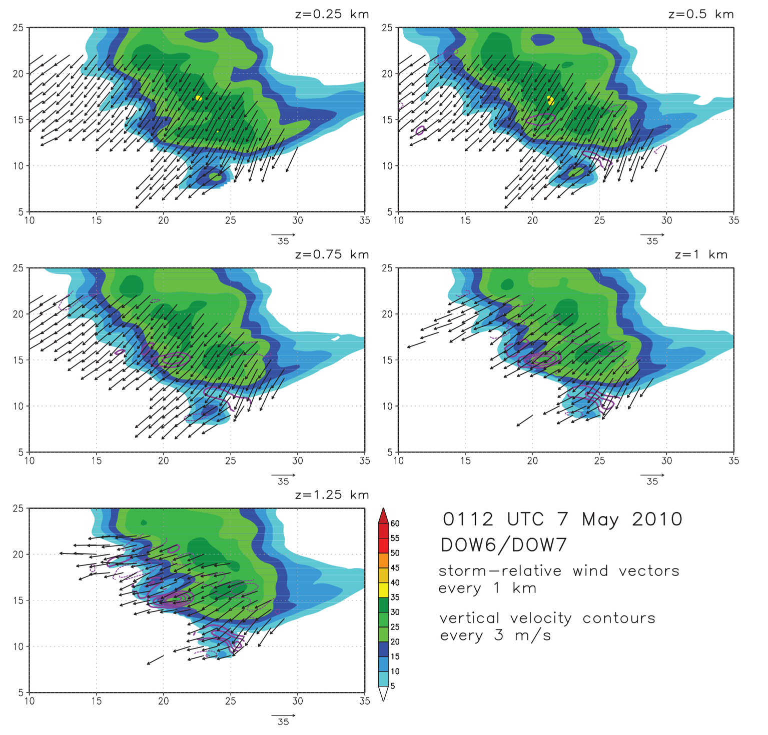

- Storm was sustained by favorable parcels from above the post-frontal stable layer (Fig. 5)
  - → Despite large CIN throughout much of the elevated layer, sufficient lifting (Fig. 5) was achieved for the supercell to be maintained well into the evening
- Shear and helicity parameters (Table 2) increased over time, providing dynamical support for supercell maintenance and aid in overcoming the large CIN
- Supercell appears to be decoupled from the stable low-level airmass, with no clear thermodynamic or kinematic boundaries (Fig. 6)
  - → Storm-scale downdrafts (i.e., rear flank downdraft, forward-flank downdraft) do not appear to reach the surface (Fig. 7)

←
Fig. 7: Horizontal cross-sections of reflectivity (shaded), storm-relative wind vectors (derived using the DOW6 and DOW7 radars and WSR-88D storm motion), and vertical velocity (contoured every 3 m/s) every 250 m through 1.25 km. The x- and y-axes represent distance in km from the center of the grid (which the the position of DOW7).

→ *15 May 2010 (dissipating supercell)*

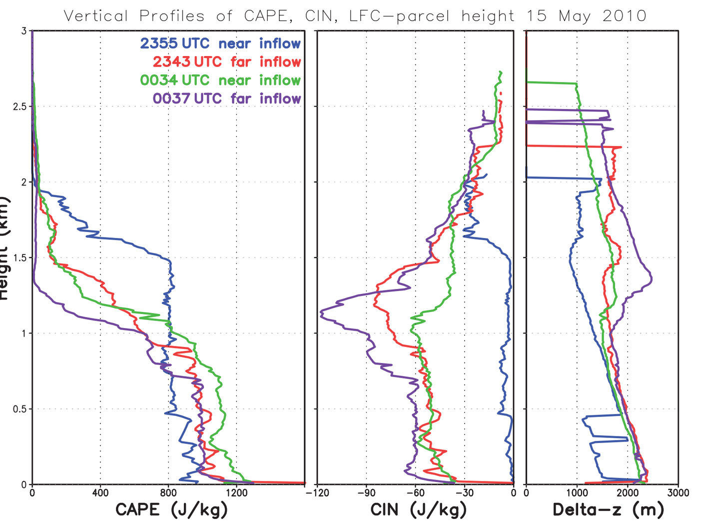

Fig. 8: As in Fig. 1, but for the inflow soundings launched on 15-16 May 2010.

Near Inflow

	2355 UTC	0034 UTC
0-6 km shear (m/s)	N/A	28.3
0-3 km shear (m/s)	N/A	19.5
0-1 km shear (m/s)	2.3	3.4
Effective shear (m/s)	N/A	10.3
0-3 km SRH (m²/s²)	N/A	154
0-1 km SRH (m²/s²)	-1	37
Effective SRH (m²/s²)	N/A	74
Effective layer depth (m)	1910	1570

Table 3: As in Table 1, but for the near inflow soundings launched on 15-16 May 2010. Note that some parameters are unavailable ("N/A") due to lost GPS signal at a low altitude.

Far Inflow

	2343 UTC	0037 UTC
0-6 km shear (m/s)	N/A	22.8
0-3 km shear (m/s)	13.6	9.7
0-1 km shear (m/s)	2.5	1.3
Effective shear (m/s)	7.9	5.7
0-3 km SRH (m²/s²)	154	123
0-1 km SRH (m²/s²)	37	35
Effective SRH (m²/s²)	84	60
Effective layer depth (m)	1520	1220

Table 4: As in Table 3, but for the far inflow soundings launched on 15-16 May 2010.

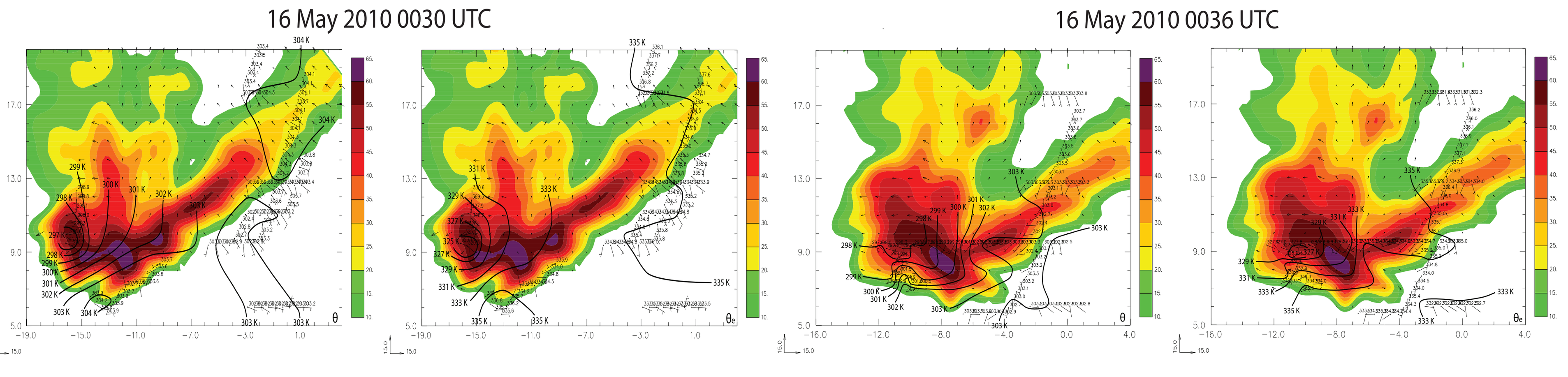

Fig. 9: As in Fig. 2, but at 0030 and 0036 UTC 16 May 2010. Dual-Doppler winds are 1 km above the ground and were derived using the UMass-XPol and NOXP radars. The x- and y-axes represent distance in km from the center of the grid (which is the position of UMXP).

- As the storm moved off of the terrain, the inflow environment was characterized by fairly constant instability but increasing inhibition and additional lifting needed to reach the LFC (Fig. 8)
  - → Orographic flows can influence stability parameters and subsequently storm evolution (e.g., Markowski and Dotzek 2011)
- The evolution of the wind profile is more difficult to ascertain, though there appears to have been only minor changes in shear and helicity (Tables 3-4)
- Storm outflow became more divergent over time, surging ahead as storm trended towards demise (Fig. 9)

Summary

- All three cases contained sufficient instability for maintenance, with varying degrees of convective inhibition present
- Increasing inhibition can be a factor leading to demise, however sufficient lifting is also important
  - → Decreasing shear and helicity on 9 June 2009 may have lead to weaker dynamic lifting; cold pool lifting may also have weakened due to low-level cooling
  - → Strong dynamical support via large shear and helicity on 6 May 2010 may have allowed an elevated supercell to persist in spite of large CIN
  - → Orographic lifting provided localized support for convective development on 15 May 2010, which likely weakened downstream of the terrain

Ongoing/Future Work

- Incorporate additional radar data to establish complete timelines of storm evolution for each case
- Numerical simulations that test the relative contributions of thermodynamic and kinematic modifications to storm demise versus persistence

Acknowledgements

The authors would like to acknowledge Conrad Ziegler for beneficial discussions concerning this research as well as the Convective Storms Group at NCSU for their assistance and feedback. Additional thanks go to the VORTEX2 PIs for making their datasets available. This research is supported by NSF under Grant ATM-0758509.